Graph theorem for chiral exact flat bands at charge neutrality

Gurjyot Sethi [1,*], Bowen Xia,[1,*] Dongwook Kim,[1] Hang Liu,[2,3] Xiaoyin Li [1] and Feng Liu [1,†]

[1]*Department of Materials Science & Engineering, University of Utah, Salt Lake City, Utah 84112, USA*
[2]*Songshan Lake Materials Laboratory, Dongguan, Guangdong 523808, People's Republic of China*
[3]*Beijing National Laboratory for Condensed Matter Physics and Institute of Physics,*
Chinese Academy of Sciences, Beijing 100190, People's Republic of China

Chiral exact flat bands (FBs) at charge neutrality have attracted much recent interest, presenting an intriguing condensed-matter system to realize exotic many-body phenomena, as *specifically* shown in magic-angle twisted bilayer graphene for superconductivity and triangulene-based superatomic graphene for exciton condensation. Yet, no *generic* physical model to realize such FBs has been developed. Here we present a mathematical theorem called bipartite double cover (BDC) theorem and prove that the BDC of line-graph (LG) lattices hosts at least two chiral exact flat bands of opposite chirality, i.e., yin-yang FBs, centered-around/at charge neutrality ($E = 0$) akin to the chiral limit of twisted bilayer graphene. We illustrate this theorem by mapping it exactly onto tight-binding lattice models of the BDC of LGs of hexagonal lattice for strong topological and of triangular lattice for fragile topological FBs, respectively. Moreover, we use the orbital design principle to realize such exotic yin-yang FBs in non-BDC lattices to instigate their real material discovery. This paper not only enables the search for exact chiral FBs at zero energy beyond moiré heterostructures but also opens the door to discovering quantum semiconductors featured with FB-enabled strongly correlated carriers.

I. INTRODUCTION

In recent years, the importance of topological flat bands (FBs) in realizing exotic many-body phenomena, such as superconductivity [1–4], excitonic superfluidity [5–8], and magnetism [2,9–11], has been highlighted through a plethora of studies [1–5,9–15] following magic-angle twisted bilayer graphene (MATBG) [1,16–21]. Lately, there has also been increasing interest in realizing the chiral limit of MATBG with topologically fragile *exact* FBs of opposite chirality at charge neutrality [22–25] using external perturbations, such as periodic strain [23]. Another intriguing case where topological FBs emerge near charge neutrality is a superatomic graphene lattice [5,26,27]. It hosts two topological strong exact FBs of opposite chirality at $E = \pm t$, i.e., the yin-yang FBs centered symmetrically at $E = 0$. These chiral exact FBs around/at charge neutrality exhibit fascinating transport properties of one-/two-body carriers due to their overlapping Wannier functions, as manifested in unconventional superconductivity for fragile topological FBs of TBG [13,28,29] and in excitonic Bose-Einstein condensation for strong topological yin-yang FBs of superatomic graphene [5,6], respectively.

Beyond these specific systems, however, no generic theory or lattice design principle for constructing exact FBs with opposite chirality around/at Fermi level has been reported yet. On the other hand, topological FBs are also known to exist in a special class of two-dimensional (2D) lattices called line-graph (LG) lattices [30–34], where the presence of at least one FB is guaranteed by mathematical LG theorem [35]. Compared to FBs at (around) $E = 0$ in MATBG (superatomic graphene), however, FBs in LG lattices are at $E = -2t$ [36], with t being the tight-binding (TB) hopping integral. Although it was shown recently that LGs of so-called split-graph lattices contain one additional FB at $E = 0$ [34], real material with split-graph lattice has rarely been found due to physically unrealistic hopping constraints.

In this paper, we present a graph theorem called bipartite double cover (BDC) theorem and prove that the BDC of LG lattices always has at least two FBs of opposite chirality around/at the Fermi level formed by bonding and antibonding pairing of the two copies of LG FB eigenfunctions, respectively. We illustrate this theorem by mapping it exactly onto realistic physical models of a TB Hamiltonian. First, we use the BDC of kagome lattice (the LG of hexagonal lattice) to show that it has two strong topological FBs of opposite chirality as the valence and conduction band edge, respectively, forming a quantum semiconductor as exemplified in the case of superatomic graphene [6]. We then show that the BDC of LG of triangular lattice has four fragile topologically exact FBs at charge neutrality, as exemplified in the case of the chiral limit of MATBG [22] but without the need of a superlattice potential or external fields. The FB topology of both BDC-LG lattices is confirmed using Chern number calculations and Wilson loop analyses. Finally, we elaborate on the effective orbital design principle [31] for chiral exact FBs, based on the symmetries of BDC-LG wave functions to find orbitals that can be placed in the non-LG lattices to overcome the hopping

---

[*]These authors contributed equally to this work.
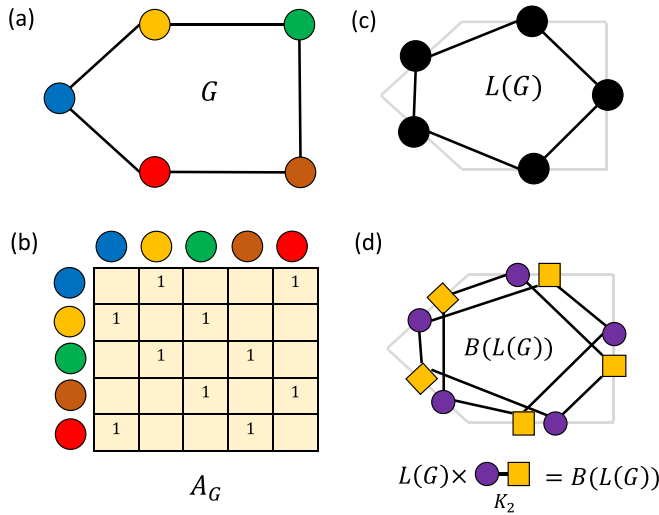[†]fliu@eng.utah.edu

035140-1

FIG. 1. (a) A finite cyclic graph (G) with five vertices indicated by colored circles and five edges indicated by black solid lines. (b) Adjacency matrix of G (A_G) with matrix element 1 between the two circles which have an edge between them. (c) Line graph of G [$L(G)$]. (d) BDC of $L(G)$ [$B(L(G))$].

constraints in the BDC-LG lattices, and hence to facilitate their material discovery.

II. LINE-GRAPH THEOREM - BIPARTITE DOUBLE COVER

In mathematics, a graph (G) consists of a set of objects with some pairs of objects coupled with each other [37], as represented by vertices (objects) and edges (pair relation) in Fig. 1(a). Each graph is assigned with an adjacency matrix (A_G) that has a matrix element of 1 to denote an adjacent pair of vertices [Fig. 1(b)]. An LG of G [$L(G)$] is constructed to depict adjacencies between the edges of G, namely, $L(G)$ is a graph, in which each vertex of $L(G)$ represents an edge of G, and the two vertices of $L(G)$ are adjacent if and only if their corresponding edges share a common vertex in G [Fig. 1(c)]. G is sometimes referred to as the root graph of $L(G)$. The LG theorem states that *the spectra of infinite LG [$L(X)$], i.e., the eigenvalues of $A_{L(X)}$ with X being an infinite graph, always has at least one lowest eigenvalue at -2 with infinite multiplicity provided the number of vertices exceeds the number of edges in the repeating unit of X* [35], which works in any dimension, including 1D lattice [31] (also see Sec. I in the Supplemental Material (SM) [38–44]).

The striking implication of the LG theorem is seen in the electronic structure of lattices based on LGs. The TB model of a lattice (L) is defined as the set of atomic sites and hopping matrix elements (t) between the sites. Each lattice can be associated with an infinite graph: A vertex set of X consisting of exactly one vertex for each lattice point, and an edge between all the vertex pairs for which $t \neq 0$. This leads to a one-to-one correspondence between a TB lattice and a mathematical graph [36],

$$H_L = tA_X, \tag{1}$$

where H_L denotes the TB Hamiltonian matrix in real space. Then, naturally, if L is based on a LG, there exists at least

one exact FB in the band structure at energy $E = -2t$. The degeneracy of the FB is given by the difference between the number of independent vertices and edges in the unit cell (SM Sec. I [38]), which can also be explained by the index theorem or sublattice imbalance between the root graph and LG [45,46]. The LG FBs can be strong or fragile topological depending on if the root graph X is bipartite or nonbipartite, respectively [34,47]. For the former, there is always a touching point between the FB and another dispersive band which can be viewed as a Berry flux center in analogy to the Dirac point [48] and be gapped out in the presence of spin-orbit coupling (SOC), leading to a strong topological quasi-FB while, for the latter, fragile exact FBs are isolated from the rest of the bands [47], also at $E = -2t$.

In graph theory, a BDC can also be constructed from a graph. BDC is one of the covering spaces of a graph, which is known to link discrete graphs to topological crystal structures [49]. BDC maps every vertex v_i of G to two (double) vertices u_i and w_i. It is called bipartite because the two vertices u_i and w_j are connected by an edge in BDC if and only if the corresponding v_i and v_j have an edge between them in G, i.e., one can divide the vertices of BDC into two independent subsets [50]. In Fig. 1(d), as an example, we show the BDC of a finite LG [$L(G)$] in Fig. 1(b), denoted by $B[L(G)]$. BDC can also be written as the tensor product of graphs, $L(G) \times K_2$, where K_2 is simply a two-vertex graph, consisting of a circle and a square in Fig. 1(d). Edges exist only between a circle and a square and only if the two corresponding black circles have an edge between them in $L(G)$ [Fig. 1(b)].

In this paper, we focus on the BDCs [$B(L(X))$] of infinite LGs [$L(X)$]. Following the BDC construction, the adjacency matrix is given by

$$A_{B(L(X))} = \begin{bmatrix} 0 & A_{L(X)} \\ A_{L(X)}^T & 0 \end{bmatrix}, \tag{2}$$

where $A_{L(X)}$ is the adjacency matrix of $L(X)$ and the basis of $A_{B(L(X))}$ is the set $\{\{u_i\},\{w_i\}\}$ or $\{\{circles\},\{squares\}\}$ so the only nonzero matrix elements are in the off-diagonal blocks. Note that $A_{L(X)}$ is always a symmetric matrix, i.e., $A_{L(X)} = A_{L(X)}^T$ [51]. Effectively, we have two copies of $L(X)$ but formed between two vertex subsets. Suppose one of the infinite eigenvectors of $A_{L(X)}$ corresponding to eigenvalue -2 is v, satisfying $A_{L(X)}v = A_{L(X)}^T v = -2v$. One can construct a vector $V = [v ; v]$ in the basis of $A_{B(L(X))}$. From Eq. (2), it is clear that V will be an eigenvector of $A_{B(L(X))}$, satisfying $A_{B(L(X))}V = -2V$. Similarly, one can construct a vector $V' = [v ; -v]$ that satisfies $A_{B(L(X))}V' = 2V'$. Note that there are infinite possible v's with eigenvalue -2 of $A_{L(X)}$, and for each of them one symmetrically (V) and one antisymmetrically (V') paired eigenvector of $A_{B(L(X))}$ can be constructed, formulating a *new* graph theorem, which we call the BDC theorem: *The spectra of BDC of infinite LGs contains at least two eigenvalues with infinite multiplicity at -2 and 2.*

One can physically understand the above theorem by carefully looking at the structure of $A_{B(L(X))}$. The absence of a matrix element between the individual elements of u_i or w_i renders the exact chiral symmetry to BDC which implies that if λ is an eigenvalue of $A_{B(L(G))}$, its opposite $-\lambda$ should also be an eigenvalue. Alternatively, note that due to the chiral nature of $A_{B(L(X))}$, its square matrix $A_{B(L(X))}^2$ would be block diagonal,
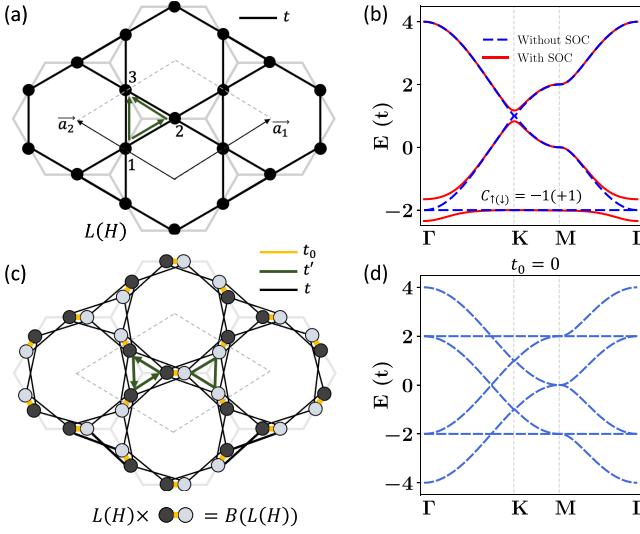
FIG. 2. (a) Line graph of hexagonal lattice [$L(H)$] where gray lines form the root graph (H) while black lines form the kagome lattice [$L(H)$]. Unit cell with three sites numbered 1–3 is depicted by gray dashed lines. Green arrows denote SOC hopping directions. (b) Band structure of (a) without (dashed blue lines) and with (solid red lines) SOC. (c) BDC construction of (a). Unit cell is depicted by gray dashed lines. Green arrows are the directions of SOC hopping. (d) Band structure of (c) with $t_0 = 0$.

given by

$$A^2_{B(L(X))} = \begin{bmatrix} A^2_{L(X)} & 0 \\ 0 & A^2_{L(X)} \end{bmatrix}. \qquad (3)$$

Now, if λ is an eigenvalue of $A_{L(X)}$, λ^2 is an eigenvalue of $A^2_{L(X)}$. From Eq. (3), it can be easily seen that λ^2 will also be an eigenvalue of $A^2_{B(L(X))}$. Then, using the property of the square-root matrix [46], the eigenvalue set of $A_{B(L(X))}$ should consist of $\{\pm\lambda\}$, implying that the spectra of $A_{B(L(X))}$ has two copies of the spectra of $A_{L(X)}$ with one inverted with respect to the other. Also, the eigenvectors corresponding to the two opposite eigenvalues are formed by the bonding ($[v;v]$) and antibonding ($[v;-v]$) pairing of the individual $L(X)$ eigenvectors. This theorem has important consequences on the electronic structure of a TB lattice associated with the BDC of a LG. It guarantees a chiral symmetric band structure having at least two FBs: one at $E = -2t$ and the other at $E = 2t$.

III. CASE STUDY I KAGOME LATTICE

To gain intuition about BDC construction and confirm the existence of two FBs in band structure, we revisit a well-known TB lattice model based on the LG of bipartite hexagonal lattice (H), i.e., kagome lattice [$L(H)$], shown in Fig. 2(a). The energy eigenspectrum of $H_{L(H)}$ is the typical kagome band structure [dashed lines in Fig. 2(b)], which has an exact FB at $E = -2t$ without SOC, in accordance with the LG theorem. Considering a spinful TB model with SOC (λ), a gap opens at the band-touching point (Γ), leading to a topologically nontrivial quasi-FB [solid lines in Fig. 2(b) at $\lambda = 0.1t$] with Chern number $C_{\uparrow(\downarrow)} = -1(+1)$. The stable/strong

topology of this FB can be confirmed by ribbon calculations where there are clear gapless edge states (Fig. S2(a) in the SM [38]).

The BDC of kagome lattice [$B(L(H))$] is constructed using the tensor product of $L(H)$ with a two-vertex graph (K_2) with dark- and light-filled circles in Fig. 2(c). To maintain the translation symmetry, K_2 is placed along specific directions. Note that the first-nearest neighbor (NN) hopping lines in $L(H)$ are transformed into third-NN hopping lines in $B(L(H))$. The TB Hamiltonian can be directly constructed using Eqs. (1) and (2), leading to chiral symmetric electronic band structure as shown in Fig. 2(d) having two exact FBs at $E = -2t$ and $E = 2t$. However, the two FBs are not near/at charge neutrality as seen in the chiral limit of TBG or diatomic kagome lattice [26]. This can be remedied by noting that the hopping between dark and light filled atomic site in $B(L(H))$ is neglected. This is because the BDC construction does not have an edge between the vertices of K_2 [Fig. 1(d)]. Physically, this is the shortest bond length in a lattice and usually has a hopping integral [t_0, yellow bonds in Fig. 2(c)] larger than the third-NN hopping (t). An important observation here is that including t_0, i.e., including an edge between the two vertices of K_2, will not alter the chiral symmetry of $A_{B(L(H))}$ since this new edge introduces only a diagonal matrix element in the off-diagonal block of $A_{B(L(H))}$. Hence, the spinless TB Hamiltonian of $B(L(H))$ with the inclusion of t_0 can be written as

$$H_{B'(L(H))} = tA_{B(L(H))} + t_0 \begin{bmatrix} 0 & I \\ I & 0 \end{bmatrix}, \qquad (4)$$

where I is identity matrix with the dimensions of the basis set of $L(H)$. The second term in Eq. (4) implies that the electronic spectrum of root $L(H)$ and of its chiral copy is shifted up- and downward by t_0, respectively, i.e., the band structure of $B'(L(H))$ has two FBs, but now at $E = -2t + t_0$, and $E = 2t - t_0$.

In Figs. 3(a) and 3(b) (dashed lines), we show the band structure obtained by diagonalizing $H_{B'(L(H))}$ with $t_0 = 2t$ and $t_0 = 3t$, respectively. For $t_0 = 2t$, there are two exact FBs completely degenerate at charge neutrality ($E = 0$), while for $t_0 = 3t$, the two FBs are gapped ($E = \pm t$), forming valence and conduction band edges. Thus, the chiral symmetric band structures are guaranteed by the BDC theorem even with the inclusion of t_0. Importantly, both FBs have a band-touching point with another dispersive band at Γ. Similar to the case of $L(H)$, they can be gapped out via SOC. A spinful Hamiltonian can be written by adding SOC effect containing positive (negative) hopping terms along (opposite to) the directions indicated by green dashed arrows in Fig. 2(c). As seen from the solid lines in Fig. 3(b), two quasi-FBs emerge with SOC having opposite chirality given by $C^{FB_c}_{\uparrow(\downarrow)} = -C^{FB_v}_{\uparrow(\downarrow)} = -1(+1)$, where $FB_{v(c)}$ indicates valence (conduction) FB. They are hence called yin-yang FBs, which have recently been shown to be an ideal platform for exotic optoelectronic properties, such as excitonic condensation [6] and giant circular dichroism [52]. We have confirmed the strong topology of these FBs using ribbon calculations (Fig. S2(b) in the SM [38]).

An interesting feature of strong topological FBs is their compact localized (plaquette) states [30], manifesting a
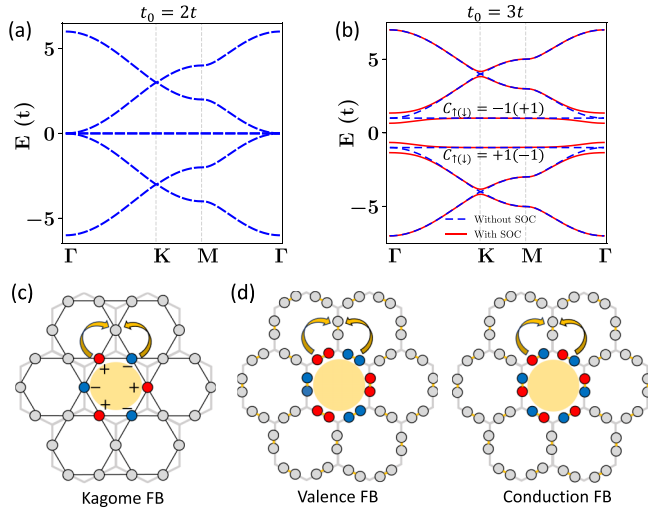
FIG. 3. (a) Band structure of Fig. 2(c) with $t_0 = 2t$ containing two exact FBs at $E = 0$. (b) Band structure of Fig. 2(c) with $t_0 = 3t$. (c) Compact localized state (CLS) for kagome FB in Fig. 2(b). (d) CLS for yin-yang valence (left) and conduction (right) FB in (b) formed by bonding and antibonding pairing of (c), respectively. Blue and red circles indicate the opposite phases of the wave functions, respectively.

completely localized FB wave function and real-space topology, as shown in Fig. 3(c) for kagome FBs. Outward hopping from the plaquette vanishes due to opposite phases of the wave function on neighboring sites that cancel each other out, leading to a destructive interference pattern. Interestingly, each of the yin-yang FBs also shows the destructive interference patterns around a plaquette, but importantly with a bonding and antibonding nature for the valence and conduction FB wave functions, respectively [26], as shown in Fig. 3(d). Here we show that this is a direct consequence of the BDC theorem

involving bonding and antibinding paring of the LG eigenfunctions.

IV. CASE STUDY II KAGOME-3 LATTICE

Next, we show the BDC construction for fragile topological FBs at charge neutrality. We consider the LG of a nonbipartite triangular (T) lattice, the so-called kagome-3 lattice [$L(T)$] [47,53] as depicted in Fig. 4(a). Similar to $L(H)$, the unit-cell of $L(T)$ also contains three sites. The difference arises in the hopping terms. In $L(T)$, in addition to NN, there are second-NN and third-NN hopping terms [Fig. 4(a)] [38], leading to a TB band structure with two exact FBs at $E = -2t$ shown in Fig. 4(b). The two FBs are fragile topological, i.e., topological obstruction to Wannier localization can be resolved by adding a trivial band [54,55]. Previous studies [47,53] have confirmed the fragile topology of these FBs using Wilson loop analysis [56], which we include in the SM [38]. An essential point to note here is that the topology of these FBs at $E = -2t$ is akin to the single-particle bands of MATBG centered/at $E = 0$ [53]. Following the procedure illustrated above for strong topological FBs, one can also construct a BDC lattice of $L(T)$ as shown in Fig. 4(c) to obtain fragile LG FBs centered/at $E = 0$. The BDC construction leads to doubled sites in the unit cell with a six-band TB Hamiltonian formulated following Eqs. (1) and (2) and the inclusion of t_0 [Eq. (4)] [38]. The band structure of $B(L(T))$ is shown in Fig. 4(d) for $t_0 = 2t$. There are four exact FBs at charge neutrality, which are fragile topological. To illustrate this, in Fig. 4(e) we calculate the Wilson loop of each spin sector separately, since the spinful time-reversal and S^z symmetries are conserved. The winding in the Wilson loop spectra of the four FBs establishes their topological nature, without SOC, with two pairs each belonging to the nontrivial Euler class $|e_2| = 1$ [57]. We next add trivial bands to the system
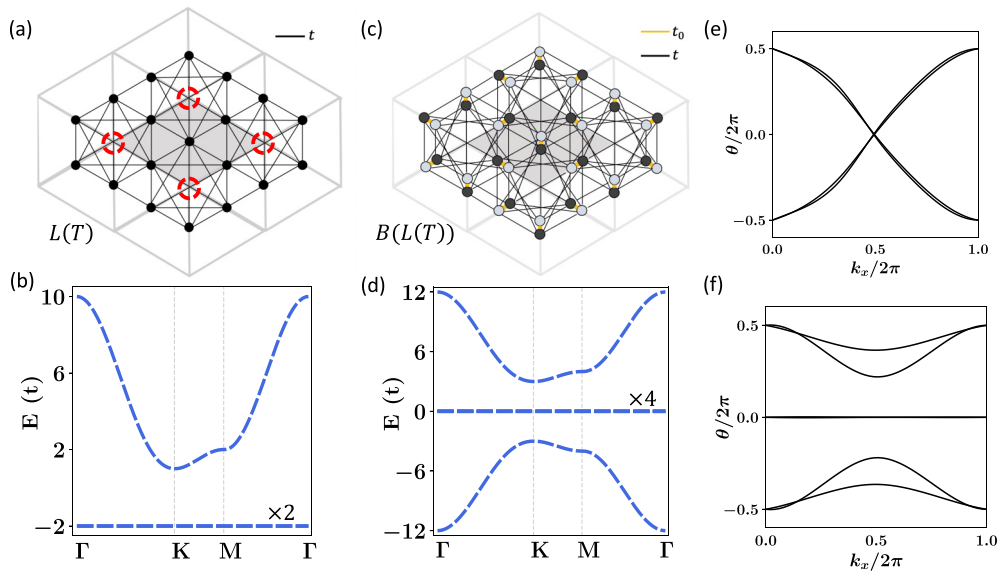

FIG. 4. (a) Kagome-3 lattice: Line-graph of triangular lattice [$L(T)$]. Dashed red circle denotes a Wycoff position. (b) Band structure of (a). (c) BDC of (a) [$B(L(T))$]. (d) Band structure of (c) with $t_0 = 2t$. (e) Wilson loop spectrum of the four FBs at charge neutrality in (d). (f) Same as (e) but with two additional s-orbitals in $B(L(T))$ at sites corresponding to the Wycoff position in (a).
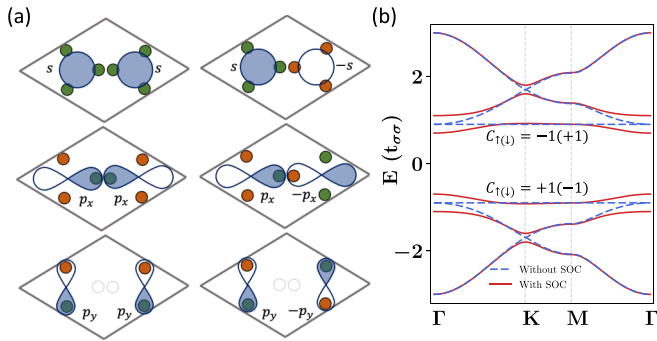
FIG. 5. (a) Six Γ-point wave functions of bands denoted by blue dashed lines in Fig. 3(b). (b) TB band structure of hexagonal lattice model with sp^2 orbitals.

by introducing an additional s orbital on the Wycoff position indicated by the red circle in Fig. 4(a) [53]. The BDC of this extended model becomes an eight-band model [38]. The Wilson loop spectra of six middle bands is shown in Fig. 4(f). The nontrivial winding of FBs is now clearly removed, confirming the fragile topology of these FBs at charge neutrality.

V. ORBITAL DESIGN OF BIPARTITE DOUBLE COVER LATTICES

Next, we notice that the BDC-LG lattice construction involves unusual hopping constraints, such as the absence of second-NN hopping term ($t' = 0$) in $B(L(H))$ [Fig. 2(c)] while requiring a nonzero third-NN hopping integral ($t \neq 0$). Realizing such peculiar hopping integrals in real materials could prove significantly challenging. On the other hand, most real materials are composed of multi-atomic orbitals on each site instead of a single s-orbital. Therefore, we finally illustrate orbital realization of chiral exact FBs of $B(L(H))$ following the procedure described in Ref. [31] that may instigate real material discovery of these exotic FBs. We first calculate the six eigenstates at Γ of the $B(L(H))$ band structure [Fig. 3(b)] and plot them in Fig. 5(a). If one groups three sites into a superatom site, then the six sites of $B(L(H))$ can be mapped onto two sites of a hexagonal lattice with three orbitals on each site. And based on the symmetry of the eigenstates, six eigenstates in Fig. 5(a) can be viewed as (s, p_x, p_x) orbitals on two hexagonal sites. Then, by choosing the two-center Slater-Koster hopping integrals [58] as $t_{ss\sigma} = 1$ eV,

$t_{sp\sigma} = 0.8t_{ss\sigma}$, $t_{pp\sigma} = 0.4t_{ss\sigma}$, in a spinless TB model [38], yin-yang FBs are reproduced as shown by dashed blue lines in Fig. 5(b). We further add the on-site SOC on p orbitals and consider a spinful model which opens a gap between dispersive band and FB [red solid lines in Fig. 5(b)]. The calculated Chern numbers for two FBs are $C^{\mathrm{FB}_c}_{\uparrow(\downarrow)} = -C^{\mathrm{FB}_v}_{\uparrow(\downarrow)} = -1(+1)$. Note that the condition $t' = 0$ in the single s-orbital model transforms into the condition $t_{pp\pi} = 0$ for the sp^2-hexagonal model. Physically, $t_{pp\pi}$ is the weakest hopping integral by symmetry. A candidate real material should be one with sp^2 frontier orbitals on hexagonal symmetric lattice but a large lattice parameter which reduces $t_{pp\pi}$. Indeed, triangulene-based superatomic graphene satisfies this condition [26] and has also been recently synthesized [59]. A similar orbital design principle can be used for other BDC-LG constructions [38].

VI. CONCLUSION

The BDC theorem, as derived and illustrated in this paper, allows for the discovery of exact FBs at charge neutrality leading to an intrinsic lattice/material [$B(L(T)$] that can realize strongly correlated physics of MATBG without the need of external fields or fine-tuning of twist angles. Moreover, we point to the possibility of an unusual quantum semiconductor in $B(L(H))$ with valence and conduction FBs (yin-yang FBs), which upon doping create FB electron and hole carriers with unique transport properties due to their nontrivial quantum metric and nonzero superfluidic weight [28,60]. This can have significant implications for the discovery and design of beyond-silicon electronic and optoelectronic devices [61]. We emphasize that our BDC design principle works for all LG lattices, both in 2D and 3D [38]. In addition, it can be easily extended to precursor-based organic materials such as triangulene crystals [62] and artificial lattice systems [63–65], where the hopping parameters can be manipulated by design. One can also consider weighted graphs with varying NN hopping integrals [36] to realize materials/models with FBs of opposite chirality. Another possible future direction could be to investigate the properties of the FBs in BDC lattices under external magnetic field [66,67].

[1] Y. Cao, V. Fatemi, S. Fang, K. Watanabe, T. Taniguchi, E. Kaxiras, and P. Jarillo-Herrero, Unconventional superconductivity in magic-angle graphene superlattices, Nature (London) **556**, 43 (2018).

[2] L. Balents, C. R. Dean, D. K. Efetov, and A. F. Young, Superconductivity and strong correlations in moiré flat bands, Nat. Phys. **16**, 725 (2020).

[3] J. M. Park, Y. Cao, K. Watanabe, T. Taniguchi, and P. Jarillo-Herrero, Tunable strongly coupled superconductivity in

magic-angle twisted trilayer graphene, Nature (London) **590**, 249 (2021).

[4] J. M. Park, Y. Cao, L.-Q. Xia, S. Sun, K. Watanabe, T. Taniguchi, and P. Jarillo-Herrero, Robust superconductivity in magic-angle multilayer graphene family, Nat. Mater. **21**, 877 (2022).

[5] G. Sethi, Y. Zhou, L. Zhu, L. Yang, and F. Liu, Flat-band-enabled triplet excitonic insulator in a diatomic Kagome lattice, Phys. Rev. Lett. **126**, 196403 (2021).

[6] G. Sethi, M. Cuma, and F. Liu, Excitonic condensate in flat valence and conduction bands of opposite chirality, Phys. Rev. Lett. **130**, 186401 (2023).

[7] G. Sethi, D. Sheng, and F. Liu, Anomalous bilayer quantum Hall effect, Phys. Rev. B **108**, L161112 (2023).

[8] X. Hu, T. Hyart, D. I. Pikulin, and E. Rossi, Quantum-metric-enabled exciton condensate in double twisted bilayer graphene, Phys. Rev. B **105**, L140506 (2022).

[9] J. Liu and X. Dai, Orbital magnetic states in moiré graphene systems, Nat. Rev. Phys. **3**, 367 (2021).

[10] C. Tschirhart, M. Serlin, H. Polshyn, A. Shragai, Z. Xia, J. Zhu, Y. Zhang, K. Watanabe, T. Taniguchi, M. Huber *et al.*, Imaging orbital ferromagnetism in a moiré Chern insulator, Science **372**, 1323 (2021).

[11] E. Y. Andrei, D. K. Efetov, P. Jarillo-Herrero, A. H. MacDonald, K. F. Mak, T. Senthil, E. Tutuc, A. Yazdani, and A. F. Young, The marvels of moiré materials, Nat. Rev. Mater. **6**, 201 (2021).

[12] Y.-H. Zhang, D. Mao, Y. Cao, P. Jarillo-Herrero, and T. Senthil, Nearly flat Chern bands in moiré superlattices, Phys. Rev. B **99**, 075127 (2019).

[13] P. Törmä, L. Liang, and S. Peotta, Quantum metric and effective mass of a two-body bound state in a flat band, Phys. Rev. B **98**, 220511(R) (2018).

[14] Y. H. Kwan, Y. Hu, S. H. Simon, and S. A. Parameswaran, Exciton band topology in spontaneous quantum anomalous Hall insulators: Applications to twisted bilayer graphene, Phys. Rev. Lett. **126**, 137601 (2021).

[15] Z.-D. Song and B. A. Bernevig, Magic-angle twisted bilayer graphene as a topological heavy fermion problem, Phys. Rev. Lett. **129**, 047601 (2022).

[16] D. M. Kennes, M. Claassen, L. Xian, A. Georges, A. J. Millis, J. Hone, C. R. Dean, D. N. Basov, A. N. Pasupathy, and A. Rubio, Moiré heterostructures as a condensed-matter quantum simulator, Nat. Phys. **17**, 155 (2021).

[17] K. F. Mak and J. Shan, Semiconductor moiré materials, Nat. Nanotechnol. **17**, 686 (2022).

[18] M. H. Naik, E. C. Regan, Z. Zhang, Y.-H. Chan, Z. Li, D. Wang, Y. Yoon, C. S. Ong, W. Zhao, S. Zhao *et al.*, Intralayer charge-transfer moiré excitons in van der Waals superlattices, Nature (London) **609**, 52 (2022).

[19] F. Wu, T. Lovorn, E. Tutuc, and A. H. MacDonald, Hubbard model physics in transition metal dichalcogenide moiré bands, Phys. Rev. Lett. **121**, 026402 (2018).

[20] R. Bistritzer and A. H. MacDonald, Moiré bands in twisted double-layer graphene, Proc. Natl. Acad. Sci. USA **108**, 12233 (2011).

[21] J. M. B. Lopes Dos Santos, N. M. R. Peres, and A. H. Castro Neto, Continuum model of the twisted graphene bilayer, Phys. Rev. B **86**, 155449 (2012).

[22] G. Tarnopolsky, A. J. Kruchkov, and A. Vishwanath, Origin of magic angles in twisted bilayer graphene, Phys. Rev. Lett. **122**, 106405 (2019).

[23] X. Wan, S. Sarkar, S.-Z. Lin, and K. Sun, Topological exact flat bands in two-dimensional materials under periodic strain, Phys. Rev. Lett. **130**, 216401 (2023).

[24] M.-R. Li, A.-L. He, and H. Yao, Magic-angle twisted bilayer systems with quadratic band touching: Exactly flat bands with high Chern number, Phys. Rev. Res. **4**, 043151 (2022).

[25] Q. Gao, J. Dong, P. Ledwith, D. Parker, and E. Khalaf, Untwisting moiré physics: Almost ideal bands and fractional Chern insulators in periodically strained monolayer graphene.

[26] Y. Zhou, G. Sethi, H. Liu, Z. Wang, and F. Liu, Excited quantum anomalous and spin Hall effect: Dissociation of flat-bands-enabled excitonic insulator state, Nanotechnology **33**, 415001 (2022).

[27] X. Ni, Y. Zhou, G. Sethi, and F. Liu, π-orbital yin–yang kagome bands in anilato-based metal–organic frameworks, Phys. Chem. Chem. Phys. **22**, 25827 (2020).

[28] P. Törmä, S. Peotta, and B. A. Bernevig, Superfluidity and quantum geometry in twisted multilayer systems, Nat. Rev. Phys. **4**, 528 (2022).

[29] J. Herzog-Arbeitman, V. Peri, F. Schindler, S. D. Huber, and B. A. Bernevig, Superfluid weight bounds from symmetry and quantum geometry in flat bands, Phys. Rev. Lett. **128**, 087002 (2022).

[30] Z. Liu, F. Liu, and Y.-S. Wu, Exotic electronic states in the world of flat bands: From theory to material, Chin. Phys. B **23**, 077308 (2014).

[31] H. Liu, G. Sethi, S. Meng, and F. Liu, Orbital design of flat bands in non-line-graph lattices via line-graph wave functions, Phys. Rev. B **105**, 085128 (2022).

[32] H. Liu, S. Meng, and F. Liu, Screening two-dimensional materials with topological flat bands, Phys. Rev. Mater. **5**, 084203 (2021).

[33] A. Mielke, Ferromagnetism in the Hubbard model on line graphs and further considerations, J. Phys. A: Math. Gen. **24**, 3311 (1991).

[34] D.-S. Ma, Y. Xu, C. S. Chiu, N. Regnault, A. A. Houck, Z. Song, and B. A. Bernevig, Spin-orbit-induced topological flat bands in line and split graphs of bipartite lattices, Phys. Rev. Lett. **125**, 266403 (2020).

[35] D. Cvetkovic, P. Rowlinson, and S. Simic, *Spectral Generalizations of Line Graphs: On Graphs with Least Eigenvalue -2* (Cambridge University Press, Cambridge, UK, 2004), Vol. 314.

[36] A. J. Kollár, M. Fitzpatrick, P. Sarnak, and A. A. Houck, Line-graph lattices: Euclidean and non-Euclidean flat bands, and implementations in circuit quantum electrodynamics, Commun. Math. Phys. **376**, 1909 (2020).

[37] D. Brent West, *Introduction to Graph Theory* (Upper Saddle River, NJ, Prentice Hall, 2001), Vol. 2.

[38] See Supplemental Material at http://link.aps.org/supplemental/10.1103/PhysRevB.109.035140 where we have included discussion regarding the relationship between incidence matrices and square-root TB models, explicit TB Hamiltonians for the cases studied in the paper, details about the wilson loop calculations, and examples of BDC construction using 2D/3D line-graph lattices, which also includes Refs. [39–44].

[39] D. Cvetkovic, M. Doob, and H. Sachs, *Spectra of graphs. Theory and Application* (Academic Press, Cambridge, Massachusetts, 1980).

[40] J. Arkinstall, M. H. Teimourpour, L. Feng, R. El-Ganainy, and H. Schomerus, Topological tight-binding models from nontrivial square roots, Phys. Rev. B **95**, 165109 (2017).

[41] T. Mizoguchi, T. Yoshida, and Y. Hatsugai, Square-root topological semimetals, Phys. Rev. B **103**, 045136 (2021).

[42] Z.-D. Song, L. Elcoro, and B. A. Bernevig, Twisted bulk-boundary correspondence of fragile topology, Science **367**, 794 (2020).

[43] A. Alexandradinata, X. Dai, and B. A. Bernevig, Wilson-loop characterization of inversion-symmetric topological insulators, Phys. Rev. B **89**, 155114 (2014).

[44] Y. Zhou, K.-H. Jin, H. Huang, Z. Wang, and F. Liu, Weyl points created by a three-dimensional flat band, Phys. Rev. B **99**, 201105(R) (2019).

[45] E. H. Lieb, Two theorems on the Hubbard model, Phys. Rev. Lett. **62**, 1201 (1989).

[46] M. Ezawa, Systematic construction of square-root topological insulators and superconductors, Phys. Rev. Res. **2**, 033397 (2020).

[47] C. S. Chiu, D.-S. Ma, Z.-D. Song, B. A. Bernevig, and A. A. Houck, Fragile topology in line-graph lattices with two, three, or four gapped flat bands, Phys. Rev. Res. **2**, 043414 (2020).

[48] D. L. Bergman, C. Wu, and L. Balents, Band touching from real-space topology in frustrated hopping models, Phys. Rev. B **78**, 125104 (2008).

[49] T. Sunada, *Topological Crystallography: With a View Towards Discrete Geometric Analysis* (Springer Science & Business Media, Japan, 2012), Vol. 6.

[50] A. S. Asratian, T. M. Denley, and R. Häggkvist, *Bipartite Graphs and Their Applications* (Cambridge University Press, Cambridge, UK, 1998), Vol. 131.

[51] N. Biggs, *Algebraic Graph Theory* (Cambridge University Press, Cambridge, UK, 1993), Vol. 67.

[52] Y. Zhou, G. Sethi, C. Zhang, X. Ni, and F. Liu, Giant intrinsic circular dichroism of enantiomorphic flat Chern bands and flatband devices, Phys. Rev. B **102**, 125115 (2020).

[53] V. Peri, Z.-D. Song, B. A. Bernevig, and S. D. Huber, Fragile topology and flat-band superconductivity in the strong-coupling regime, Phys. Rev. Lett. **126**, 027002 (2021).

[54] H. C. Po, L. Zou, T. Senthil, and A. Vishwanath, Faithful tight-binding models and fragile topology of magic-angle bilayer graphene, Phys. Rev. B **99**, 195455 (2019).

[55] H. C. Po, H. Watanabe, and A. Vishwanath, Fragile topology and Wannier obstructions, Phys. Rev. Lett. **121**, 126402 (2018).

[56] B. Bradlyn, Z. Wang, J. Cano, and B. A. Bernevig, Disconnected elementary band representations, fragile topology, and wilson loops as topological indices: An example on the triangular lattice, Phys. Rev. B **99**, 045140 (2019).

[57] J. Ahn, S. Park, and B.-J. Yang, Failure of Nielsen-Ninomiya theorem and fragile topology in two-dimensional systems with space-time inversion symmetry: Application to twisted bilayer graphene at magic angle, Phys. Rev. X **9**, 021013 (2019).

[58] J. C. Slater and G. F. Koster, Simplified LCAO method for the periodic potential problem, Phys. Rev. **94**, 1498 (1954).

[59] A. Delgado, C. Dusold, J. Jiang, A. Cronin, S. G. Louie, and F. R. Fischer, Evidence for excitonic insulator ground state in triangulene kagome lattice, arXiv:2301.06171.

[60] J. Herzog-Arbeitman, A. Chew, K.-E. Huhtinen, P. Törmä, and B. A. Bernevig, Many-body superconductivity in topological flat bands, arXiv:2209.00007.

[61] K. H. Jin, W. Jiang, G. Sethi, and F. Liu, Topological quantum devices a review, Nanoscale **15**, 12787 (2023).

[62] R. Ortiz, G. Catarina, and J. Fernández-Rossier, Theory of triangulene two-dimensional crystals, 2D Mater. **10**, 015015 (2023).

[63] K. Dong, T. Zhang, J. Li, Q. Wang, F. Yang, Y. Rho, D. Wang, C. P. Grigoropoulos, J. Wu, and J. Yao, Flat bands in magic-angle bilayer photonic crystals at small twists, Phys. Rev. Lett. **126**, 223601 (2021).

[64] D. Leykam, A. Andreanov, and S. Flach, Artificial flat band systems: From lattice models to experiments, Adv. Phys.: X **3**, 1473052 (2018).

[65] V. Apaja, M. Hyrkäs, and M. Manninen, Flat bands, Dirac cones, and atom dynamics in an optical lattice, Phys. Rev. A **82**, 041402(R) (2010).

[66] H. Aoki, M. Ando, and H. Matsumura, Hofstadter butterflies for flat bands, Phys. Rev. B **54**, R17296 (1996).

[67] A. M. Marques, J. Mögerle, G. Pelegrí, S. Flannigan, R. G. Dias, and A. J. Daley, Kaleidoscopes of Hofstadter butterflies and Aharonov-Bohm caging from 2^n-root topology in decorated square lattices, Phys. Rev. Res. **5**, 023110 (2023).